Heliyon

Received:
16 September 2016
Revised:
12 December 2016
Accepted:
5 January 2017

Cite as: Joseph M. Mannion, Matthew S. Wellons, Charles R. Shick, Glenn A. Fugate, Brian A. Powell, Scott M. Husson. Ambient aging of rhenium filaments used in thermal ionization mass spectrometry: Growth of oxo-rhenium crystallites and anti-aging strategies. Heliyon 3 (2017) e00232. doi: 10.1016/j.heliyon.2017.e00232

Ambient aging of rhenium filaments used in thermal ionization mass spectrometry: Growth of oxo-rhenium crystallites and anti-aging strategies

Joseph M. Mannion [a], Matthew S. Wellons [b], Charles R. Shick [b], Glenn A. Fugate [b,1], Brian A. Powell [c], Scott M. Husson [a,*]

[a] *Department of Chemical and Biomolecular Engineering, Clemson University, 127 Earle Hall, Clemson, SC 29634, USA*

[b] *Savannah River National Laboratory, National Security Directorate, Aiken, SC 29808, USA*

[c] *Department of Environmental Engineering and Earth Sciences, Clemson University, 342 Computer Court, Anderson, SC 29625, USA*

* Corresponding author.

E-mail address: shusson@clemson.edu (S.M. Husson).

[1] Present address: Oak Ridge National Laboratory, Nuclear Security & Isotope Technology Division, Oak Ridge, TN 37831, USA.

Abstract

Degassing is a common preparation technique for rhenium filaments used for thermal ionization mass spectrometric analysis of actinides, including plutonium. Although optimization studies regarding degassing conditions have been reported, little work has been done to characterize filament aging after degassing. In this study, the effects of filament aging after degassing were explored to determine a "shelf-life" for degassed rhenium filaments, and methods to limit filament aging were investigated. Zone-refined rhenium filaments were degassed by resistance heating under high vacuum before exposure to ambient atmosphere for up to 2 months. After degassing the nucleation and preferential growth of oxo-rhenium crystallites on the surface of polycrystalline rhenium filaments was observed by

http://dx.doi.org/10.1016/j.heliyon.2017.e00232

atomic force microscopy and scanning electron microscopy (SEM). Compositional analysis of the crystallites was conducted using SEM-Raman spectroscopy and SEM energy dispersive X-ray spectroscopy, and grain orientation at the metal surface was investigated by electron back-scatter diffraction mapping. Spectra collected by SEM-Raman suggest crystallites are composed primarily of perrhenic acid. The relative extent of growth and crystallite morphology were found to be grain dependent and affected by the dissolution of carbon into filaments during annealing (often referred to as carbonization or carburization). Crystallites were observed to nucleate in region specific modes and grow over time through transfer of material from the surface. Factors most likely to affect the rates of crystallite growth include rhenium substrate properties such as grain size, orientation, levels of dissolved carbon, and relative abundance of defect sites; as well as environmental factors such as length of exposure to oxygen and relative humidity. Thin (~180 nm) hydrophobic films of poly(vinylbenzyl chloride) were found to slow the growth of oxo-rhenium crystallites on the filament surfaces and may serve as an alternative carbon source for filament carburization.

Keywords: Materials Science

1. Introduction

Rhenium has been used widely as an ionization surface in thermal ionization mass spectrometry (TIMS) for isotopic analysis of plutonium [1, 2]. Rhenium is the preferred material in these analyses for its high work function and melting point that is well above ionization temperatures for plutonium [3]. Rhenium also has been employed as an ionization surface for a variety of other analytes [4, 5, 6, 7, 8]. The use of rhenium in other high-temperature applications has been limited by its oxidation characteristics [9]. It readily oxidizes above 600 °C when exposed to atmospheric oxygen and water vapor [10, 11]. High vacuum, thus low oxygen partial pressure, environments produced in TIMS systems are what enable the successful use of rhenium as a thermal ionization filament. Despite its susceptibility to oxidation and terrestrial scarcity, rhenium has remained an important material in the production of turbine blades [12], catalysts [13], and heating elements [14]; consequently, rhenium has been the subject of scientific investigations for many decades [15, 16, 17, 18, 19, 20, 21, 22, 23]. Despite these efforts, little is known about the chemical identities of species involved in catalytic [24] and surface ionization mechanisms [25, 26] due to the challenges associated with *in-situ* analysis.

Over decades of use in TIMS systems, various pretreatment methods for rhenium filaments have been developed to improve ionization efficiency [7, 27, 28, 29]. The most common of these pretreatment methods is known as “degassing” or “outgassing” of filaments prior to sample loading and analysis. Degassing involves

http://dx.doi.org/10.1016/j.heliyon.2017.e00232

resistively heating the filaments under high vacuum for a specified duration of time. Degassing generally is performed to reduce isobaric interferences and background signals that arise from contaminants within the rhenium filaments [30, 31]. Filament contaminants are volatilized during the degassing treatment due to the high temperature and ultralow pressure. Studies have sought to optimize this process by monitoring the background signals of particular contaminants produced by blank rhenium filaments after various degassing conditions [32].

An additional effect of degassing is that it drives oxides of rhenium off of the ionization surface prior to sample loading. The oxidation behavior of polycrystalline rhenium surfaces is complex due in part to the large number of oxidation states exhibited by rhenium [33], shifts in O-Re binding energy arising from non-local interactions with neighboring oxides [34, 35], and the propensity for high energy anisotropic planes of the hexagonal close packed surface to undergo oxygen-induced meta-stable morphological transformations [36, 37]. The binary oxides of rhenium at near ambient pressures are ReO_4, Re_2O_7, ReO_3, and ReO_2 containing rhenium in the VIII, VII, VI, and IV oxidation states. The vaporization temperatures of these oxides are reported to be 220, 362, 614, and 1362 °C respectively [38]. ReO_3 is reported to undergo disproportionation to ReO_2 and Re_2O_7 between 400 and 537 °C, and ReO_2 disproportionates to Re metal and Re_2O_7 between 850 and 1077 °C [39]. Filament currents used for resistive heating during degassing are often similar to those used during analysis to ensure that volatile compounds released at sample ionization temperatures are driven from the filaments prior to sample loading. It has been estimated that filaments reach ~1500 °C at a current of 3.5 A [32]. In the case of plutonium analyses, it can be expected that filament temperatures reached during degassing are >1500 °C [30, 40, 41].

The motivation for this work was to determine a "shelf life" for degassed rhenium filaments. Experience at Savannah River National Laboratory (SRNL) suggests that decreased analytical performance can be expected when low level plutonium samples are loaded onto filaments exposed to atmosphere for more than approximately 30 days. Despite the commonality of degassing within the TIMS community, no direct study involving the effects of filament aging could be found in the literature. Additionally, studies involving ambient atmospheric aging of rhenium surfaces over relatively long durations of time are absent in the literature. In this study, surface conditions of rhenium filaments subjected to long-term aging in atmosphere were monitored to gain insights to understand the observations made at SRNL. Additionally, methods and storage conditions that may limit the effects of atmospheric aging were investigated in an effort to extend the "shelf life" of degassed filaments. This paper reports findings regarding the discovery of an unreported rhenium oxidation behavior: the nucleation and preferential growth of nano- to micro-scale oxo-rhenium crystallites on polycrystalline metallic rhenium surfaces under ambient conditions. The efficacies of coating the filaments with

http://dx.doi.org/10.1016/j.heliyon.2017.e00232

ultra-thin polymer films and filament carburization as a means to slow the growth of these oxides were also investigated. Although the viewpoint that filament aging negatively impacts TIMS analyses remains anecdotal, the consistency of this observation across the TIMS community lends confidence and merits further investigation. In this paper we propose that surface oxidation contributes to filament aging and propose mechanisms by which these oxides may negatively impact TIMS analyses.

2. Materials and methods

2.1. Materials

The following materials were obtained from Sigma-Aldrich and used as-received: chloroform (Reagent Plus® ≥ 99.8% with 0.5–1.0% ethanol as stabilizer, CAS# 67-66-3) and poly(vinylbenzyl chloride) (PVBC), 60/40 mixture of 3- and 4- isomers (CAS# 121961-20-4). Rhenium ribbons were zone refined rhenium from H. Cross Company (0.762 × 0.030 mm).

2.2. Degassing and carbonation of rhenium ribbons

Rhenium strips were cut (0.762 × 0.030 × 15.9 mm) and spot welded onto posts for electrical heating. Each sample filament was heated incrementally from 0.5 Amps to 3.8 Amps in a degasser vacuum chamber at a pressure of around 10^{-5} Pa. Filaments were held at 3.8 Amps for approximately 1 h before incrementally reducing filament temperature. In cases where carburization was performed, degassed filaments were first allowed to cool before xylene vapors were introduced to the vacuum system. Once a pressure of 10^{-3} Pa was reached through the introduction of xylene, filaments were heated incrementally from 0.5 Amps to 2.0 Amps and held for approximately 20 min at 2.0 Amps in the presence of xylene vapor.

2.3. Atmospheric exposure

After removing ribbons from mounts and securing to SEM grids, ribbons were allowed to age in covered polystyrene petri dishes under atmospheric conditions. Samples were covered to prevent dust build-up.

2.4. Thin polymer film formation

After degassing, filament assemblies were dip-coated from solutions of PVBC in chloroform. Film thickness depends on polymer concentration and withdrawal rate [42]. To produce a film with a thickness of approximately 180 nm, the substrate was withdrawn from a 2 wt% PVBC solution at a withdrawal rate of 340 mm/min

http://dx.doi.org/10.1016/j.heliyon.2017.e00232

using a Qualtecs Product Industry QPI-128 dip coater. Film thicknesses were determined with multi-angle ellipsometry.

2.5. Determination of film thicknesses

Film thicknesses were measured by multi-angle, single wavelength ellipsometry (Beaglehole Instruments, Picometer). Silicon wafers were used as surrogate substrates for thickness determination, as the geometry and roughness of rhenium filaments made direct measurements on filaments by ellipsometry unreliable. The incident beam was produced by a 632.8 He-Ne laser source. Measurements were done at incidence angles from 62° to 80° with a step increment of 3°. The reported thickness is an average of five random locations on each wafer. Reported uncertainties represent ±1 standard deviation. In this study, a PVBC-silicon dioxide-silicon substrate three-layer model was applied to fit the data. PVBC thickness and refractive index based on a Cauchy model were allowed to vary and were calculated by IgorPro Software v4.0A.

2.6. Atomic force microscopy

Atomic force microscopy (AFM) images were obtained using a Bioscope AFM (Bruker, Inc.) with NanoScope III A controller. Silicon cantilevers (MikroMasch, Inc., NSC15/Si3N4/AIBS/50) were used as probes for the tapping mode measurements. AFM images were taken with 256 × 256 pixel resolution over areas of 1–10,000 μm^2 at scan rates of 0.25–1.0 Hz.

2.7. SEM/SEM-Raman/SEM-energy dispersive X-ray spectroscopy/electron back-scatter diffraction

SEM analyses were performed on a Hitachi S4800High Resolution SEM at Clemson University. Ribbons were removed from mounts used for degassing and secured to SEM grids with carbon tape. SEM-Raman and SEM energy dispersive X-ray spectroscopy (SEM/EDS) were performed at SRNL. SEM/EDS also was performed at Clemson University on a Hitachi SU6600 Variable Pressure SEM. A 785 nm laser and 30 s acquisition time were used for Raman analysis. Electron back-scatter diffraction (EBSD) mapping was performed at Clemson University on a nanoDUE'T double beam microscope NB5000.

3. Results

Zone-refined flat rhenium ribbon was cut and spot-welded onto posts for electrical resistance heating at SRNL. In this study, degassing parameters are based upon those used at SRNL for the isotopic analysis of ultra-low-level plutonium samples (~3.5 A, $\sim 10^{-5}$ Pa). Fig. 1 shows images collected by AFM of a polycrystalline rhenium surface before and shortly after degassing. Prior to degassing, rhenium

http://dx.doi.org/10.1016/j.heliyon.2017.e00232

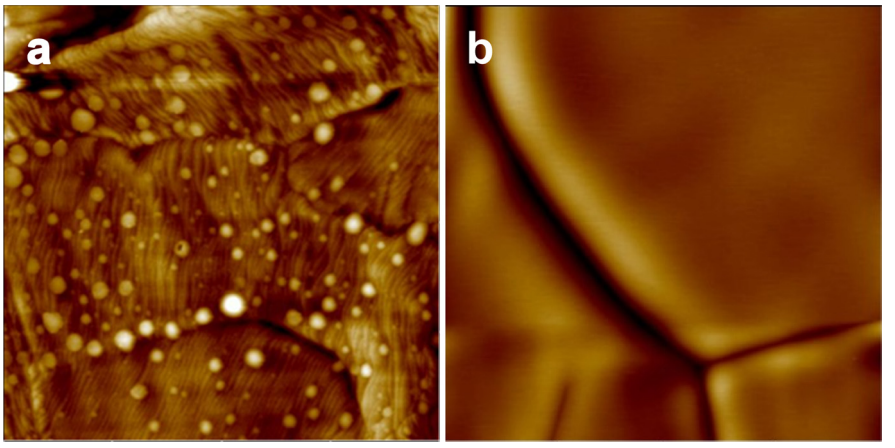

Fig. 1. AFM images of rhenium surface (a) before degassing and (b) after degassing (<1 week atmospheric exposure). Scale is 10 μm × 10 μm. Height scale is 200 nm for image (a) and 250 nm for image (b).

surfaces were found to be rough and possessed a variety of morphological features including surface ridges, mounds, and ill-defined grain boundaries, seen in Fig. 1a. The extent of atmospheric exposure experienced by these samples prior to degassing is unknown. Fig. 1b shows the rhenium surface shortly after degassing. Morphological features witnessed prior to degassing (Fig. 1a) were absent; surfaces had comparatively smooth grain surfaces and clearly defined, well-formed grain boundaries. These surfaces were monitored intermittently over the course of 1 month of aging under atmospheric conditions after degassing, during which the in-growth of surface protrusions was detected via AFM. The size and coverage of the protrusions were found to be grain dependent, making direct measurements of temporal growth by AFM difficult. Grain dependent growth of surface protrusions was supported with observations made by SEM and can be seen in Fig. 2a. After approximately 2 weeks of atmospheric exposure, densely covered grains were found that were surrounded by relatively bare, protrusion-free grains. Upon closer

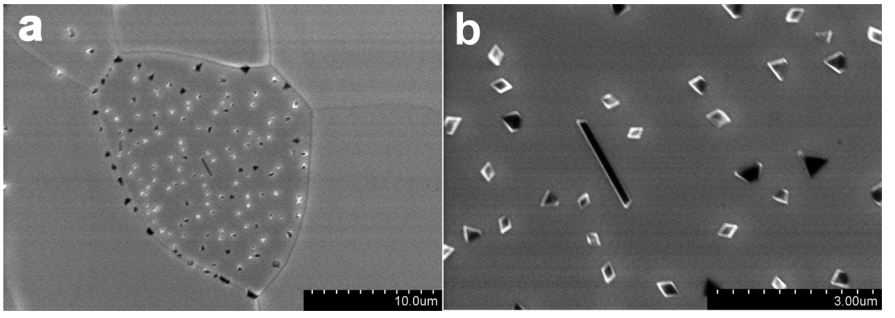

Fig. 2. SEM images of polycrystalline rhenium filament surface after approximately 2 weeks of atmospheric exposure: (a) In-growth of surface protrusions was found to be grain dependent. (b) Surface protrusions were found to be crystallites.

http://dx.doi.org/10.1016/j.heliyon.2017.e00232

inspection with SEM, these surface protrusions, which appeared as lumps or mounds on the AFM due to broadening from probe artifacts, were found to be crystallites (Fig. 2b). After longer periods of atmospheric exposure (approximately 5 weeks), significant crystallite growth was found on most surface grains; however, crystallite nucleation density and average crystallite size varied and appeared to be grain dependent (shown in Fig. 3). These initial studies performed at Clemson University were confirmed by similar analyses on an independent set of aged rhenium filament samples at SRNL. Measurements made after approximately 1 month of atmospheric exposure indicated that crystallite sizes ranged from $<$100 nm up to several microns (long axis).

Elemental mapping of these surfaces by SEM/EDS demonstrated a clear correlation between crystallite location and elevated concentrations of oxygen, seen in Fig. 4. Rhenium, carbon, and nitrogen spectral mappings showed substantially less correlation with the location of crystallites than that of oxygen; though, some correlation can be noted in spectral mapping of nitrogen. Identification of the oxo-rhenium species present in the crystallites was attempted through SEM-Raman analysis. Measurements on small crystallites were difficult due to sublimation; however, spectra were collected successfully from crystallites larger than ~1 μm. These spectra were compared with those reported for binary rhenium oxide species and were found to correlate with Re_2O_7 [43] (Fig. 5). The spectra were then compared with those for perrhenic compounds, as perrhenic acid is the hydration product of Re_2O_7, and strong correlation was found with those

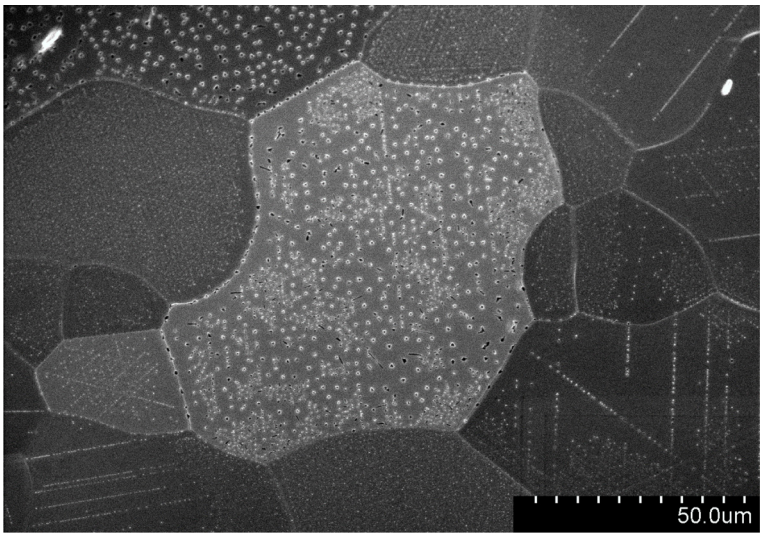

Fig. 3. SEM image of rhenium filament surface after approximately 1 month of atmospheric exposure. Crystallites were found to be present on most grains; though, inter-granular differences were noted including crystallite size, abundance, and growth patterns.

http://dx.doi.org/10.1016/j.heliyon.2017.e00232

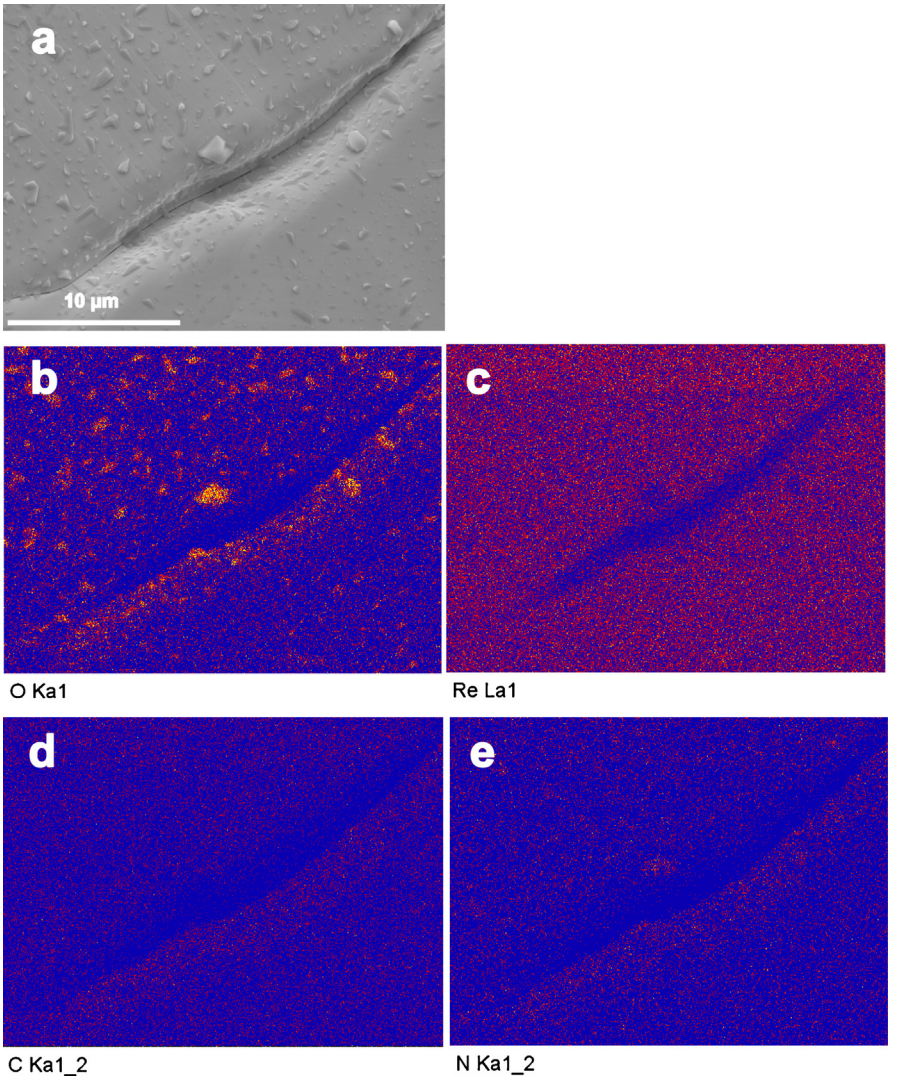

Fig. 4. SEM/EDS mapping of polycrystalline Re surface demonstrates correlation between crystallite locations and elevated oxygen. Colors in b–e indicate elemental abundance on a blue–yellow scale representing low and high abundance respectively. (a) orginal SEM image of interrogated region of filament surface. (b) mapping of oxygen showing highest level of correlation with crystallite locations, (c) rhenium, (d) carbon, and (e) nitrogen.

reported for perrhenic acid [44, 45] (Fig. 5); a comparison of Raman shifts for crystallites and those reported in literature for perrhenic acid can be seen in Table 1. Differences in spectra collected from surface crystallites and bulk samples from the literature can be attributed to surface effects, crystal orientation, and weak signal intensity. Tetragonal crystalline forms were common among crystallites observed by SEM, seen in Fig. 6. Re_2O_7 is reported to crystallize in the orthorhombic crystalline form [46]; whereas perrhenic acid has been shown to crystalize in the tetragonal system [47, 48], further supporting SEM-Raman identification of the crystallites as perrhenic in nature.

http://dx.doi.org/10.1016/j.heliyon.2017.e00232

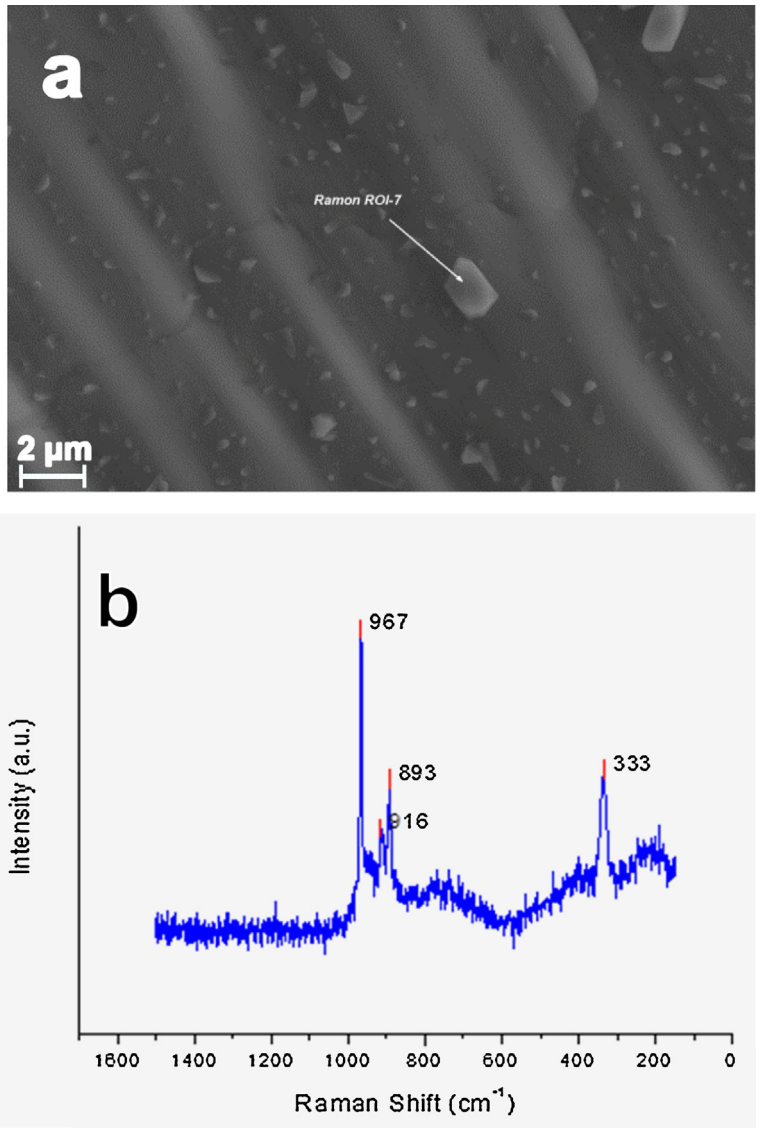

Fig. 5. SEM-Raman spectra collected from micron sized crystallites that grow on the Re surface: (a) relatively large crystallite (>1 µm) selected for analysis due to issues with sublimation of small crystallites (b) Raman spectrum collected from individual crystallite.

SEM and EBSD mapping images were collected 2 and 7 weeks after degassing rhenium samples to understand the orientation of grains and monitor the in-growth of rhenium oxide phases. The data indicate that shortly after degassing, the surfaces are composed primarily of Re metal phase with some occurrences of a ReC phase (Fig. 7a). Measurements of crystalline orientation indicate that the surfaces are dominated by the [0001] basal plane with minimal differences among grains with respect to the measured z-component of the Euler angle (Fig. 7b). Isolated grains were imaged that deviated from this basal surface orientation (Fig. 7c); however, these misoriented grains account for a small fraction of the

http://dx.doi.org/10.1016/j.heliyon.2017.e00232

Table 1. Raman shifts for crystallites and those reported in literature for perrhenic acid.

Crystallites (this study)	Perrhenic acid with assignment [45]	
967 (s)	961 (s)	ENTITYNOTDEFINED!!!1_s Re-O
916 (m)	928 (w)	ENTITYNOTDEFINED!!!3_{as} Re-O
893 (m)	891 (m)	ENTITYNOTDEFINED!!!3_{as} Re-O
	375 (w)	ENTITYNOTDEFINED!!!4 O-Re-O
		ENTITYNOTDEFINED!!!O-Re-O
333 (b/s)	337 (w)	ENTITYNOTDEFINED!!!2 O-Re-O

overall surface and therefore cannot be entirely responsible for the surface heterogeneity seen after extended periods of atmospheric exposure (~4 weeks).

Four region-specific modes of crystallite growth were identified by SEM examination of these polycrystalline rhenium surfaces: 1) growth along grain boundaries, 2) growth along linear surface dislocations, 3) random growth within relatively flat and defect-free planes, and 4) growth upon defect sites or faceted regions. The first three modes of crystallite growth can be seen in Fig. 8a, defect growth can be seen in Fig. 8b, and growth upon a faceted grain can be seen in Fig. 8c. It is unclear at this time whether crystallites migrate or diffuse from their

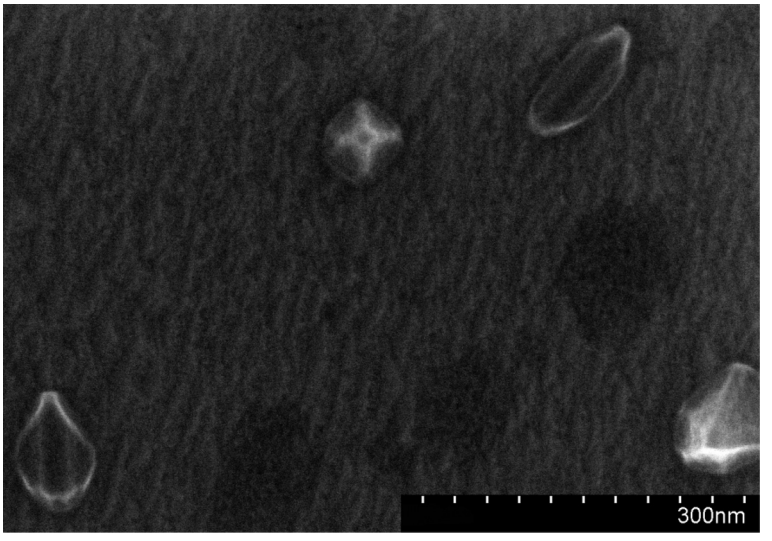

Fig. 6. Crystallites appear to be predominately tretragonal in form, and 4-fold axis and 2-fold tetragonal dipyramidal axes of symmetry can be seen directed outward from the surface.

http://dx.doi.org/10.1016/j.heliyon.2017.e00232

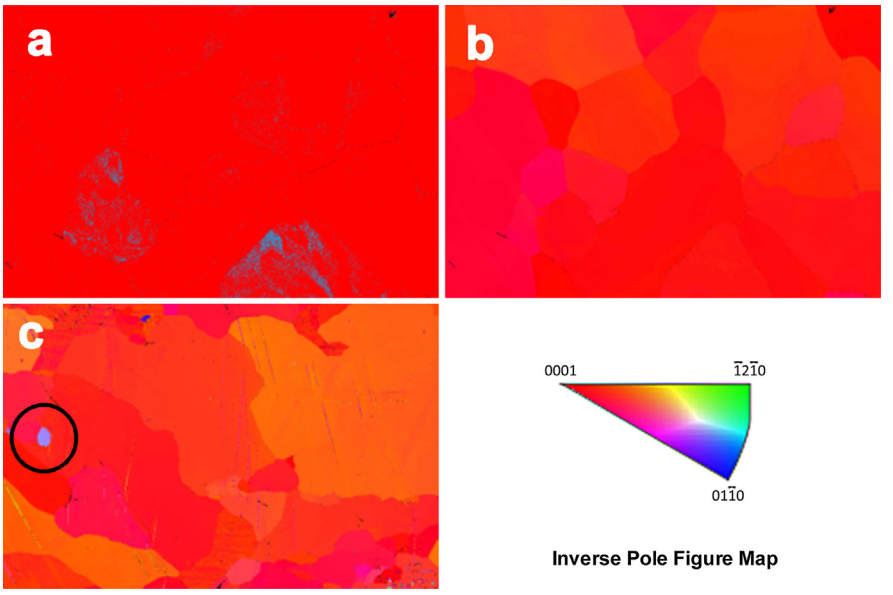

Fig. 7. EBSD mapping of polycrystalline rhenium surface: (a) Phase mapping with red indicating metallic rhenium and blue indicating rhenium-carbide (of note: these filaments were not intentionally carburized and the source of carbon is unknown at this time.) (b) z-component of Euler angle for basally oriented region. Colors relate to crystalline orientation outlined by inverse pole figure map above with the basal [0001] orientation in red. (c) z-component of Euler angle for region possessing an isolated misaligned grain seen in blue (circled in black to highlight this grain). Colors relate to crystalline orientation outlined by inverse pole figure map.

point of nucleation. Crystallite growth along linear surface dislocations was found to be common and results in the formation of crystallite lines, seen in Fig. 9a. Within a grain these crystallite lines often are parallel; however, misalignment with crystallite lines on neighboring grains (Fig. 9b) indicates these linear surface dislocations are not a direct artifact of tooling.

Fig. 10 shows SEM images of filaments exposed to atmosphere for years (exact duration unknown) in covered containers. The images suggest that after long periods of ambient atmospheric exposure, the surface crystallites grow in size and eventually begin to fuse creating a confluent coating. This theory is supported by the discovery of fused crystallites on samples exposed to atmospheric conditions for only 1 month, seen in Fig. 10b and c. In some regions of the highly aged samples (multiple years of atmospheric exposure), the confluent coating appeared to have flaked off revealing a relatively smoother subsurface. It is unclear if this loss of portions of the oxide over-layer is due to spallation or another cause.

The oxidation characteristics of carburized (a.k.a. carbonized) filaments also were investigated. Carburization procedures are incorporated into some TIMS sample preparations and involve resistance heating of the filaments under high vacuum in the presence of a carbon source. In this study, xylene vapor was injected into a

http://dx.doi.org/10.1016/j.heliyon.2017.e00232

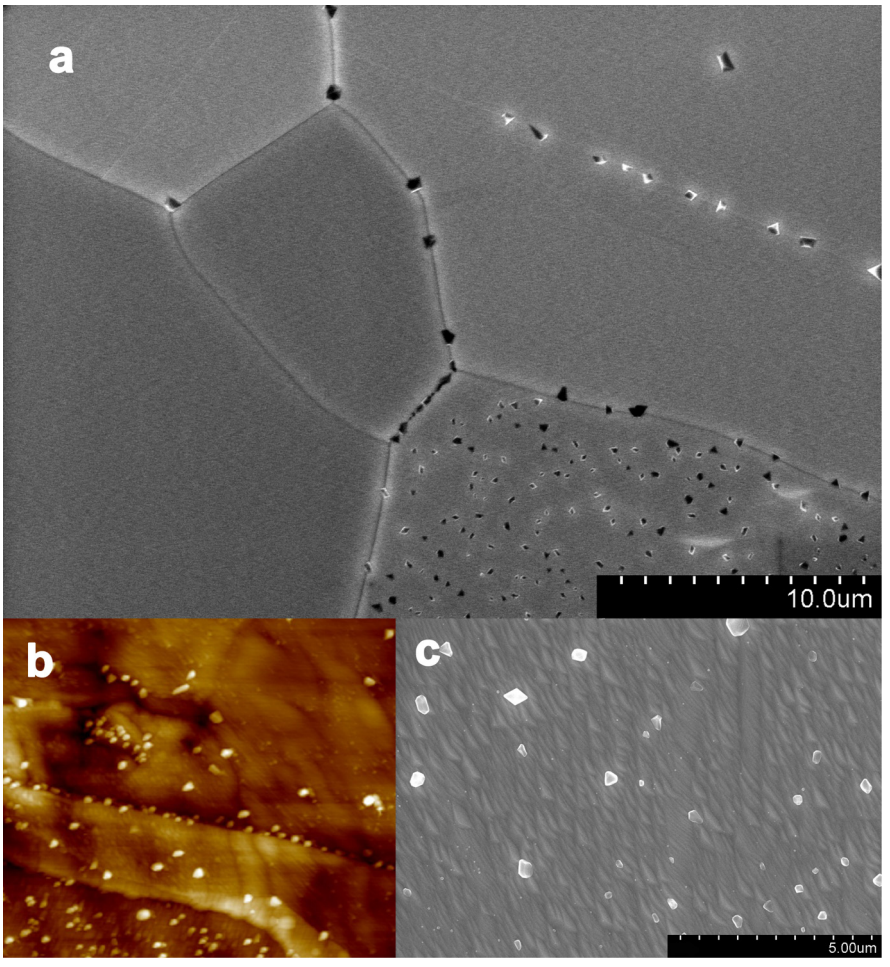

Fig. 8. (a) SEM image of surface region displaying (1) growth along grain boundaries, (2) growth along a linear surface dislocation. (3) growth within a flat plane. (b) AFM image displaying growth at defect sites (and other modes) [scale is 5 μm × 5 μm, height scale is 100 nm]. (c) SEM image of crystallite growth upon a faceted plane.

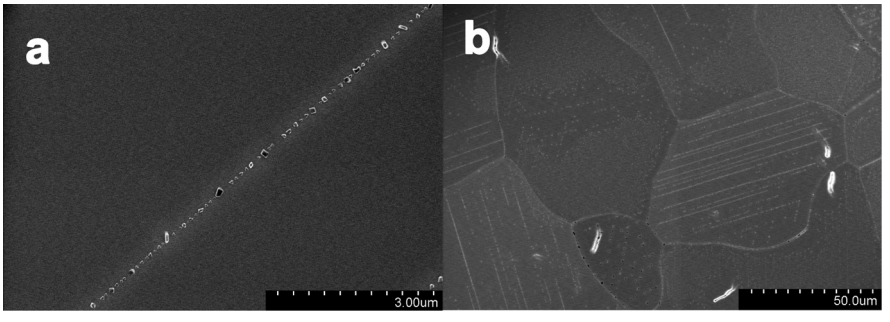

Fig. 9. SEM images of (a) crystallite growth along a linear surface dislocation and (b) collection of grains exhibiting growth along parallel linear surface dislocation (of note: growth lines are parallel within a grain but not among neighboring grains).

http://dx.doi.org/10.1016/j.heliyon.2017.e00232

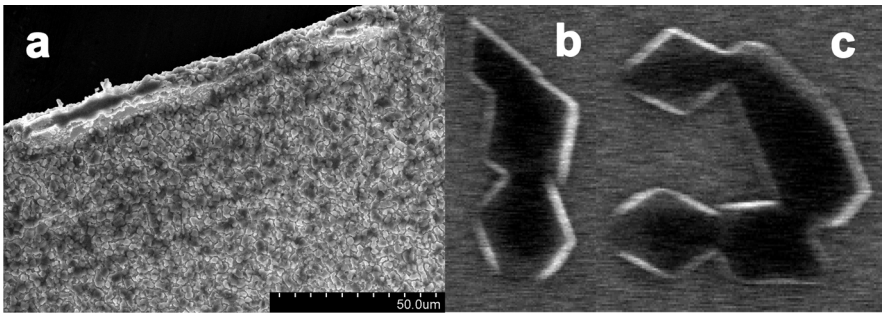

Fig. 10. (a) Highly aged sample (multiple years of atmospheric exposure) showing that the crystals continue to grow and merge to entirely cover the rhenium surface. (b, c) fused crystallites found on surface after approximately 1 month of atmospheric exposure.

custom-built degassing chamber. Carburized filaments were exposed to ambient conditions alongside filaments that had undergone no carburization process during degassing. Fig. 11 compares 120° three-point grain intersections found on carbonized and non-carbonized filaments after approximately 1 month of atmospheric exposure. Numerous differences can be noted: (1) Carbonized ribbons possess generally more defects near the grain boundaries than non-carbonized ribbons. (2) Average crystallite sizes were smaller on carbonized ribbons than non-carbonized ribbons. (3) Small gray, non-crystalline spots can be seen on carbonized ribbons that appear to be concentrated on particular grains. SEM-Raman suggests that these non-crystalline spots are carbonaceous deposits (a broad peak between 1350–1550 cm^{-1} was detected in these regions, data not shown).

The efficacy of hydrophobic thin polymer films as a means of passivating filament surfaces was investigated. Within 1 week of degassing, rhenium filaments were coated with a ~180 nm film of poly(vinylbenzyl chloride) (PVBC) by dip-coating. These coated filaments were then exposed to atmospheric conditions for 3 months,

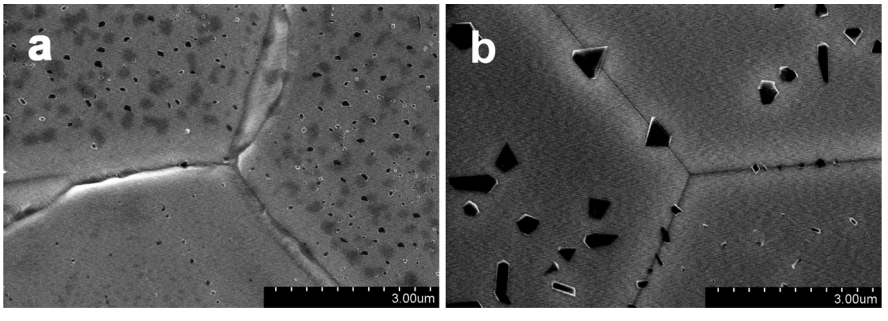

Fig. 11. Comparison of carbonized rhenium ribbons (a) and non-carbonized rhenium ribbons (b). Carbonized ribbons have a rougher surface with more defects near the grain boundaries than non-carbonized ribbons. Crystallites generally are smaller on carbonized ribbons than non-carbonized ribbons at equivalent durations of atmospheric exposure. Graphitic deposits seen as small dark spots appear on carbonized ribbons and are concentrated on particular crystalline planes.

http://dx.doi.org/10.1016/j.heliyon.2017.e00232

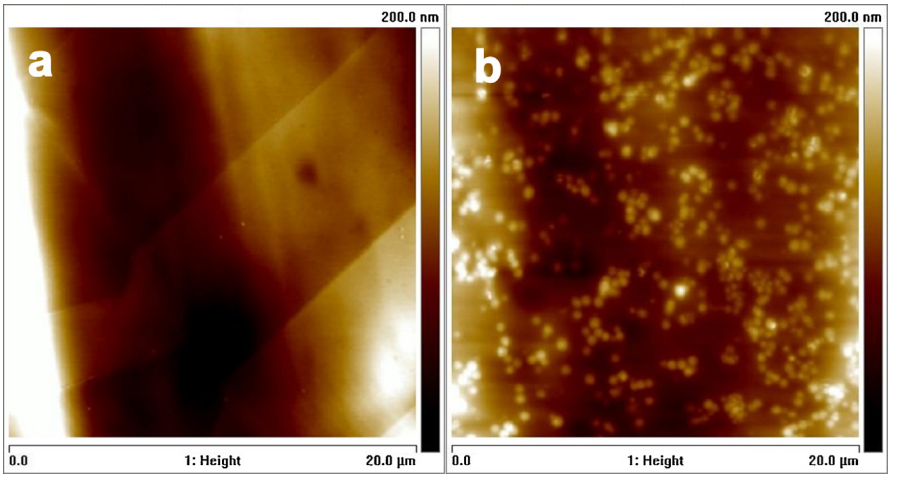

Fig. 12. AFM images of thin polymer film coated filaments. (a) Re filament coated with 180 nm film after ~1 week oxidation in atmosphere, then exposed to atmosphere for more than 3 months. (b) Re filament oxidized in atmosphere for 1 month and then coated with 500 nm film.

during which the in-growth of crystallites was absent. AFM was used for these analyses rather than SEM to prevent degradation of the thin polymer coating. Fig. 12a shows a coated filament surface after 3 months of atmospheric aging. To ensure that the polymer coating was not obscuring the visualization of any crystallites, filaments aged for 1 month in atmosphere were coated with a thicker (~500 nm) layer of polymer and imaged via AFM. It was known that these filament surfaces possessed a significant coverage of crystallites at the time of coating. Crystallites under the 500 nm film were clearly visible through AFM imaging, appearing as mounds, and can be seen in Fig. 12b. This control experiment validates the observation that thin polymer films passivate the surface to oxidation.

4. Discussion

The initial motivation for this study was the desire to determine a "shelf-life" for degassed rhenium filaments used in TIMS analysis and identify methods to extend this shelf-life. Observations made at SRNL suggest that decreased analytical performance can be expected when ultra-low-level plutonium samples are loaded onto filaments exposed to atmosphere for longer than approximately 1 month. Surface ionization mechanisms are poorly understood under conditions presented by many TIMS sample preparation schemes, and the effects of filament aging on surface conditions largely have been unexplored in the literature. It is well known that TIMS sample preparations are generally difficult, time-consuming, and costly [28]. Extending the shelf-life of rhenium filaments post-degassing could reduce the time associated with TIMS analysis by enabling bulk production of degassed rhenium filaments, thus improving sample throughput and expanding the general

http://dx.doi.org/10.1016/j.heliyon.2017.e00232

utility and feasibility of TIMS analyses. The effects and mechanisms involved in long-term ambient oxidation of polycrystalline rhenium surfaces must be understood to rationally achieve these goals.

The formation of oxo-rhenium crystallites on polycrystalline metallic rhenium surfaces appears to be limited by yet-to-be determined kinetic factors, possibly including adsorption, dissociation, nucleation, crystallization, and surface diffusion. Crystallite growth appears to progress for years, becoming significant in terms of surface coverage within 1 month of ambient atmospheric exposure after high temperature annealing under vacuum. SEM/Raman analysis suggests that crystallites are composed of perrhenic acid, which is consistent with the tetrahedral crystalline forms observed by SEM. Perrhenic acid, $Re_2O_7(H_2O)_2(s)$, is produced through the hydration of Re_2O_7. The in-growth of perrhenic acid crystals on degassed rhenium surfaces after atmospheric exposure likely is a multistage process involving: (1) the adsorption/dissociation of atmospheric oxygen (2) the oxidation of metallic rhenium to Re_2O_7, (3) the adsorption of atmospheric water vapor, and (4) the hydration of Re_2O_7 to $Re_2O_7(H_2O)_2(s)$. Factors related to the nucleation and growth of crystallites also must be considered if a predictive kinetic model is to be developed. Nucleation of these crystallites appears to be region-selective: 1) along grain boundaries, 2) along linear surface dislocations, 3) randomly within flat planes, and 4) upon defect sites or facets. Crystallite growth rates appear to correlate with these regions. Due to varying growth rates and differences in the potential extent of growth among the regions, the dominant mode of growth (in terms of surface coverage) transitions over time. Crystallite growth along grain boundaries was found to be a dominant mode for degassed samples after intermediate (1–2 weeks) levels of atmospheric exposure (Fig. 12a). After longer exposure times (4–5 weeks) crystallite growth at grain boundaries is a minor contributor to overall crystallite surface coverage (Fig. 3). Determination of a dominant mode of growth at a given point in time is thus dependent upon the average grain size of the polycrystalline surface. Temporal growth of these crystallites is evident, indicating that some transfer of material occurs between the surface and crystallites. The mechanism involved in the transfer of material from the surface is not clear at this point.

Crystallite growth along grain boundaries was pervasive among samples and occurred more rapidly than other modes of growth. This finding was somewhat expected as grain boundaries are preferred corrosion sites in many systems [49]. It is unclear at this time if crystallites formed at grain boundaries are capable of diffusing from their point of nucleation. Based on the atmospheric conditions and the average grain size of filaments used in this study, surface crystallite coverage resulting from of intra-granular modes of oxidation exceeded coverage resulting from growth at grain boundaries between 2 to 4 weeks of atmospheric exposure.

http://dx.doi.org/10.1016/j.heliyon.2017.e00232

Intra-granular growth modes were found to progress at a slower rate than crystallite growth at grain boundaries for most crystal grains; however, notable exceptions were identified by SEM (Fig. 12b) and AFM where isolated grains were found to be highly oxidized compared to neighboring grains and the surface as a whole. It was theorized that the preferential oxidation of certain grains may be due to grain orientation at the surface with some particular orientations possessing a greater propensity for ambient oxidation. However, EBSD mapping of the filament surfaces after degassing and short-term atmospheric exposure (<1 week) indicates that these surfaces are dominated the basal (0001) plane with minor incidence of other grain orientations. These low-occurrence grains, highlighted in Fig. 13, cannot account for all of the heterogeneity witnessed across these surfaces at more mature levels of crystallite growth (Fig. 3).

Among intra-granular modes of growth, crystallization along linear surface dislocations appears to be the inceptive mode of growth for many of the observed grains. The result can be seen within multiple grains in Fig. 3, where parallel lines of crystallites traverse otherwise barren intra-granular regions. This inceptive growth along dislocations may catalyze or further nucleate crystallite growth within smooth intra-granular regions of the surface; although, this hypothesis has not been tested. Growth within flat intra-granular regions was found to be the

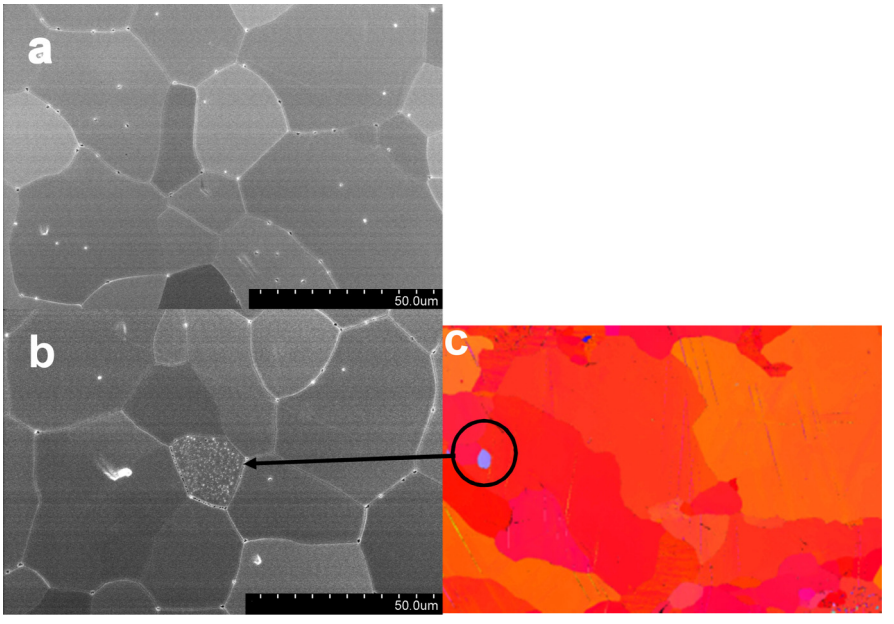

Fig. 13. (a) Basally oriented region displaying predominately growth along grain boundaries after ~2 weeks of atmospheric exposure. (b) Isolated grain found to be covered in a high density of crystallites after ~2 weeks of atmospheric exposure surrounded by relative barren grains. (c) EBSD mapping of polycrystalline surface where an isolated non-basal grain was discovered. (Of note: (b) and (c) are not the same region of the surface, these figures are intended to demonstrate a possible correlation.).

http://dx.doi.org/10.1016/j.heliyon.2017.e00232

slowest mode of growth for most grains. The relative rate of growth on faceted grains and defect sites was difficult to determine due to the low occurrence of these features on degassed samples; however, it can be inferred that growth at these sites would likely be more rapid than growth within flat intra-granular regions as was witnessed with growth along grain boundaries and linear surface dislocations. Thus, the overall rate of crystallite growth on a given surface should depend in part upon the relative abundance of these non-planar features. Processes that reduce the roughness of filament surfaces are therefore expected to reduce the rate of oxide growth upon these surfaces. The use of higher degassing temperatures leading to greater filament annealing may be a relatively simple means to acquire smoother surfaces and slow oxidation.

The incorporation of carbon through carburization procedures has been shown to increase the effective work function of polycrystalline rhenium [1, 40, 50], and changes in the effective work function of metallic surfaces can be related to changes in the redox potential of surfaces [51]. Qualitative observations by SEM suggest that at a given level of atmospheric exposure the average crystallite size is significantly smaller on rhenium surfaces that were subjected to carburization procedures than those that were degassed in the absence of a carbon source (Fig. 11). Carburization of filaments (or simply carbon incorporation) has been credited with benefiting TIMS analysis by: 1) facilitating formation of actinide carbides that stabilize actinide analytes on filament surfaces to high temperatures, increasing ionization efficiency; 2) maintaining a reducing environment on the surface of the filament, promoting the production of metallic ions and suppressing analyte-oxide formation; and 3) increasing the work function of the filaments, which increases ionization efficiency. Findings within this study suggest that carburization also increases the "shelf life" of filaments used in TIMS analysis. We hypothesize that the observed passivation afforded by carburization is due to an increase in the work function of these surfaces, which increases the activation barrier for oxidation.

The application of thin (~180 nm nominally; this thickness does not account for the filling of grain boundaries or defect regions) hydrophobic polymer coatings onto freshly degassed filaments was found to increase the "shelf life" of rhenium surfaces by limiting the formation crystallites, seen via AFM imaging in Fig. 12a. Rhenium filaments known to have a significant coverage of crystallites (aged 1 month in atmosphere with no polymer coating or carburization) were coated with a thicker (~500 nm) film of PVBC, seen in Fig. 12b. Crystallites can be seen clearly underneath the 500 nm coating in Fig. 12b, indicating that a polymer over-coat does not obfuscate AFM imaging of crystallites. PVBC was selected as the coating material in this study for its chemical similarity to Dowex anion exchange resins, commonly used in bead loading methods, and its hydrophobicity. It is unclear at this point if passivation of these coated surfaces is due to reduced oxygen diffusion,

http://dx.doi.org/10.1016/j.heliyon.2017.e00232

reduced exposure to water, or a combination thereof. Dip-coating was selected as the film formation method for its simplicity and applicability to complex substrate geometries, such as filament assemblies. In related, unpublished work, thin films of PVBC were found to be non-interfering with TIMS analysis of plutonium and serve as an alternative carbon source for low-level measurement of plutonium.

We hypothesize that the specific effects surface oxidation has on TIMS analyses will be, at least in part, dependent upon the method of sample loading. For example, a common means of performing ultra-low-level plutonium analysis includes the use of small (40–100 μm diameter) anion-exchange resin beads to concentrate and load samples [52]. The resin beads loaded with Pu are glued directly to the rhenium ionization filament after degassing. Excessive crystallite growth may interfere with adhesion of the beads to the surface. Large crystallites may prevent initial contact with the surface during preparation, leading to larger thermal gradients during the "ramp up" phase of analysis, in turn leading to sample detachment. Finally, relatively large masses of vaporizing oxides may cause a loss of adhesion. In the case of direct loading, melting and vaporization of oxides may result in sample loss from sputtering or entrainment of the sample during heating. Additionally, we hypothesize that surface oxides may negatively affect all forms of TIMS analysis through two common mechanisms. Firstly, the presence of vaporizing oxides within the ion source may lead to sample oxidation, either through direct interaction with rhenium oxides or through interaction with water after dehydration of $Re_2O_7 2(H_2O)$. Secondly, interaction with perrhenic acid may lead to the formation of plutonium perrhenate, altering the ionization and vaporization characteristics of the sample. Further investigation is needed to quantify and elucidate and the nature of interactions between vaporizing oxides and the sample within ion sources. Due to the differences in the manifestation of these negative effects we propose two metrics for future studies quantitatively evaluating the impact of filament oxidation: 1) the rate of total sample loss and 2) deviations in the expected ionization efficiency.

The identification of the oxide crystallites as perrhenic acid has an important implication in that storage humidity is expected to influence the rate of crystallite ingrowth. Variance in atmospheric humidity may in part account for inter-laboratory discrepancies in the shelf life of TIMS filaments, where it has been reported anecdotally that dry conditions lead to longer shelf lives. Due to the likely influence of humidity it is not possible to compare filaments based solely on equivalent durations of aging. Future studies on the impact of filament oxidation therefore must account for the actual quantity of surface oxides present at the time of analysis, not simply the duration of filament aging.

The authors were unable to find mention of this phenomenon in the open literature and welcome any corrections regarding the originality of these findings.

http://dx.doi.org/10.1016/j.heliyon.2017.e00232

5. Conclusions

The long-term exposure of polycrystalline rhenium surfaces to ambient air was investigated and preferential ingrowth of oxo-rhenium crystallites was observed. Crystalline form, SEM/Raman vibrational spectroscopy, and SEM/EDS support identification of these crystallites as perrhenic acid, the product of Re_2O_7 hydration. Factors known to influence the rate of crystallite ingrowth include (1) average grain size due to preferential growth at grain boundaries, (2) grain orientation, (3) relative abundance of defect sites, and (4) length of exposure to oxygen. Controlling these factors may increase shelf lives of degassed rhenium filaments used in TIMS analyses. In addition, on the basis that rhenium filament surface oxidation degrades the ionization performance, filament carburization and polymer coating techniques can be used to extend the shelf life of filaments. Polymer coatings appear to slow oxidation to a greater degree than carburization, though, the magnitude of this difference is yet to be quantified. Further investigation is needed to fully elucidate the mechanisms involved in the anecdotally observed degradation of performance when TIMS analyses are conducted with aged filaments.

Declarations

Author contribution statement

Joseph Mannion, Matthew Wellons, Charles Shick, Jr.: Conceived and designed the experiments; performed the experiments; analyzed and interpreted the data; contributed reagents, materials, analysis tools or data; wrote the paper.

Glenn Fugate, Brian Powell, Scott Husson: Conceived and designed the experiments; analyzed and interpreted the data; contributed reagents, materials, analysis tools or data; wrote the paper.

Competing interest statement

The authors declare no conflict of interest.

Funding statement

This work was supported by U.S. National Nuclear Security Administration NA-221 Office of Proliferation Detection ward No. DE-NA0001735.

Additional information

No additional information is available for this paper.

http://dx.doi.org/10.1016/j.heliyon.2017.e00232

Acknowledgements

The authors thank Taghi Darroudi and other members of the Clemson University Electron Microscopy Laboratory for their assistance with SEM, SEM/EDS, and EBSD analysis described in this work.

References

[1] P.G. Pallmer, R.L. Gordon, M.J. Dresser, The work function of carburized rhenium, J. Appl. Phys. 51 (7) (1980) 3776–3779.

[2] D. Suzuki, et al., Direct isotope ratio analysis of individual uranium-–plutonium mixed particles with various U/Pu ratios by thermal ionization mass spectrometry, Appl. Radiat. Isot. 96 (2015) 52–56.

[3] M.H. Studier, E.N. Sloth, L.P. Moore, The chemistry of uraxium in surface ionizatiox sources, J. Phys. Chem. 66 (1) (1962) 133–134.

[4] M. Touboul, R.J. Walker, High precision tungsten isotope measurement by thermal ionization mass spectrometry, Int. J. Mass Spectrom. 309 (2012) 109–117.

[5] J. Lintelmann, M.H. França, E. Hübner, G. Matuschek, A liquid chromatography-atmospheric pressure photoionization tandem mass spectrometric method for the determination of azaarenes in atmospheric particulate matter, J. Chromatogr. A 52 (4) (1980) 1636–1646.

[6] S. Mialle, et al., The use of total evaporation method using Channeltron electron multipliers by thermal ionization mass spectrometry for europium isotope ratio measurements on picogram sample amounts, Int. J. Mass Spectrom. 309 (2012) 141–147.

[7] M. Kraiem, et al., Development of an improved method to perform single particle analysis by TIMS for nuclear safeguards, Anal. Chim. Acta 688 (1) (2011) 1–7.

[8] D. Wielandt, M. Bizzarro, A TIMS-based method for the high precision measurements of the three-isotope potassium composition of small samples, J. Anal. At. Spectrom. 26 (2) (2011) 366–377.

[9] C. Duriez, Rhenium oxidation by steam at high temperatures, Oxid. Met. 61 (1–2) (2004) 49–67.

[10] J.R. Davis, ASM Specialty Handbook: Heat-Resistant Materials, ASM International, 1997, 2017.

[11] W.L. Phillips, The rate of oxidation of rhenium at elevated temperatures in air, J. Less-Common Met. 5 (1962) 97–100.

 http://dx.doi.org/10.1016/j.heliyon.2017.e00232

[12] D. Konitzer, S. Duclos, T. Rockstroh, Materials for sustainable turbine engine development, MRS Bull. 37 (04) (2012) 383–387.

[13] K. Bouchmella, et al., Olefin metathesis with mesoporous rhenium–silicium-–aluminum mixed oxides obtained via a one-step non-hydrolytic sol–gel route, J. Catal. 301 (2013) 233–241.

[14] B.D. Bryskin, Evaluation of properties and special features for high-temperature applications of rhenium, AIP Conf. Proc. 246 (1) (1992) 278–291.

[15] R. Levi, G.A. Espersen, Preparation of rhenium emitters and measurements of their thermionic properties, Phys. Rev. 78 (3) (1950) 231–234.

[16] A.U. Blackham, R.R. Beishline, L.S. Merrill, Rhenium as a catalyst in hydrocarbon reforming reactions, Ind. Eng. Chem. Prod. Res. Dev. 4 (4) (1965) 269–273.

[17] W.S. Greenlee, M.F. Farona, Olefin metathesis by rhenium carbonyl halide-alkylaluminum halide catalysts. Direct evidence for a coordinated carbene initiated process, Inorg. Chem. 15 (9) (1976) 2129–2134.

[18] R. Burch, The oxidation state of rhenium and its role in platinum-rhenium reforming catalysts, Platinum Met. Rev. 22 (2) (1978) 57–60.

[19] N.D. Spencer, G.A. Somorjai, Rhenium: an ammonia synthesis catalyst, J. Phys. Chem. 86 (18) (1982) 3493–3494.

[20] J.H. Sinfelt, Structure of bimetallic clusters, Acc. Chem. Res. 20 (4) (1987) 134–139.

[21] J.C. Mol, Olefin metathesis over supported rhenium oxide catalysts, Catal. Today 51 (2) (1999) 289–299.

[22] E.L. Kunkes, et al., The role of rhenium in the conversion of glycerol to synthesis gas over carbon supported platinum–rhenium catalysts, J. Catal. 260 (1) (2008) 164–177.

[23] G. Beamson, et al., Selective hydrogenation of amides using bimetallic Ru/Re and Rh/Re catalysts, J. Catal. 278 (2) (2011) 228–238.

[24] S. Koso, Y. Nakagawa, K. Tomishige, Mechanism of the hydrogenolysis of ethers over silica-supported rhodium catalyst modified with rhenium oxide, J. Catal. 280 (2) (2011) 221–229.

[25] D.M. Wayne, et al., The thermal ionization cavity (TIC) source: elucidation of possible mechanisms for enhanced ionization efficiency, Int. J. Mass Spectrom. 216 (1) (2002) 41–57.

 http://dx.doi.org/10.1016/j.heliyon.2017.e00232

[26] M.G. Watrous, J.E. Delmore, Metal dicarbides as intermediate species in thermal ion formation mechanisms, Int. J. Mass Spectrom. 286 (1) (2009) 7–10.

[27] M. Kraiem, et al., Filament chemistry of uranium in thermal ionisation mass spectrometry, J. Anal. At. Spectrom. 25 (7) (2010) 1138–1144.

[28] R. Jakopic, et al., Determination of 240Pu/239Pu, 241Pu/239Pu and 242Pu/239Pu isotope ratios in environmental reference materials and samples from Chernobyl by thermal ionization mass spectrometry (TIMS) and filament carburization, J. Anal. At. Spectrom. 25 (6) (2010) 815–821.

[29] R. Jakopič, et al., Certified reference materials and reference methods for nuclear safeguards and security, J. Environ. Radioact. 125 (2013) 17–22.

[30] C.-G. Lee, et al., Simultaneous determination of plutonium and uranium isotope ratios in individual plutonium–uranium mixed particles by thermal ionization mass spectrometry, Int. J. Mass Spectrom. 314 (2012) 57–62.

[31] K.J. Mathew, et al., Total evaporation method for uranium isotope-amount ratio measurements, J. Anal. At. Spectrom. 28 (6) (2013) 866–876.

[32] J.-H. Park, I.-H. Choi, K.-S. Song, A technique to minimize impurity signal from blank rhenium filaments for highly accurate TIMS measurements of uranium in ultra-trace levels, Mass Spectrom. Lett. 1 (1) (2010) 17–20.

[33] N.R. Murphy, et al., Optical and chemical properties of mixed-valent rhenium oxide films synthesized by reactive DC magnetron sputtering, Opt. Mater. 45 (2015) 191–196.

[34] A. Chan, et al., Surface atom core-level shifts of clean and oxygen-covered Re (123$\bar{1}$), Phys. Rev. B 72 (3) (2005) 035442.

[35] E. Miniussi, et al., Non-local effects on oxygen-induced surface core level shifts of Re(0001), J. Phys. Chem. C 116 (44) (2012) 23297–23307.

[36] H. Wang, W. Chen, T.E. Madey, Morphological evolution in oxygen-induced faceting of Re (123$\bar{1}$, Phys. Rev. B 74 (20) (2006) 205426.

[37] H. Wang, et al., Facet stability in oxygen-induced nanofaceting of Re (123$\bar{1}$, ACS Nano 1 (5) (2007) 449–455.

[38] M. Bai, et al., Preparation of ultrafine rhenium powders by CVD hydrogen reduction of volatile rhenium oxides, Trans. Nonferrous Met. Soc. China 23 (2) (2013) 538–542.

[39] P.A. Shcheglov, D.V. Drobot, Heterogeneous equilibria in the rhenium-oxygen system, Russ. J. Phys. Chem. 80 (11) (2006) 1819–1825.

http://dx.doi.org/10.1016/j.heliyon.2017.e00232

[40] R. Jakopič, et al., Isotope ratio measurements of pg-size plutonium samples using TIMS in combination with multiple ion counting and filament carburization, Int. J. Mass Spectrom. 279 (2–3) (2009) 87–92.

[41] C.-G. Lee, et al., Ultra-trace analysis of plutonium by thermal ionization mass spectrometry with a continuous heating technique without chemical separation, Talanta 141 (2015) 92–96.

[42] J. Zhou, et al., Formation and characterization of perfluorocyclobutyl polymer thin films, J. Appl. Polym. Sci. 129 (6) (2013) 3226–3236.

[43] H.S. Lacheen, P.J. Cordeiro, E. Iglesia, Isolation of rhenium and ReOx species within ZSM5 channels and their catalytic function in the activation of alkanes and alkanols, Chem. Eur. J. 13 (11) (2007) 3048–3057.

[44] H.H. Claassen, A.J. Zielen, Structure of the perrhenate ion, J. Chem. Phys. 22 (4) (1954) 707–709.

[45] E. Cazzanelli, et al., Characterization of rhenium oxide films and their application to liquid crystal cells, J. Appl. Phys. 105 (11) (2009) 114904.

[46] B. Krebs, A. Mueller, H.H. Beyer, Crystal structure of rhenium(VII) oxide, Inorg. Chem. 8 (3) (1969) 436–443.

[47] G. Wltschek, I. Svoboda, H. Fuess, The crystal structure of solid perrhenic acid monohydrate, Zeitschrift für anorganische und allgemeine Chemie 619 (10) (1993) 1679–1681.

[48] C.J.L. Lock, G. Turner, A reinvestigation of the crystal structure of potassium perrhenate, Acta Crystallogr. Sect. B 31 (6) (1975) 1764–1765.

[49] G.R. Argade, S.K. Panigrahi, R.S. Mishra, Effects of grain size on the corrosion resistance of wrought magnesium alloys containing neodymium, Corr. Sci. 58 (2012) 145–151.

[50] P.G. Pallmer, R.L. Gordon, M.J. Dresser, The emissivity of carburized rhenium, J. Appl. Phys. 51 (3) (1980) 1798–1801.

[51] H. Gerischer, W. Ekardt, Fermi levels in electrolytes and the absolute scale of redox potentials, Appl. Phys. Lett. 43 (4) (1983) 393–395.

[52] S. Bürger, et al., Uranium and plutonium analysis of nuclear material samples by multi-collector thermal ionisation mass spectrometry: quality control, measurement uncertainty, and metrological traceability, Int. J. Mass Spectrom. 311 (2012) 40–50.

 http://dx.doi.org/10.1016/j.heliyon.2017.e00232